END

FILMED

DTIC

| | 1.0 | |
|---|---|---|
| | 1.1 | |
| | 1.25 | 1.4 | 1.6 |

4.5 5.0 5.5 6.3

2.8 2.5
3.2 2.2
3.6
4.0 2.0
1.8

MICROCOPY RESOLUTION TEST CHART

)ARDS-1963-A

AD-A157 132

**Naval Ocean Research and Development Activity**

NSTL, Mississippi 39529     NORDA Report 93     April 1985

# Data Analysis of Airborne Electromagnetic Bathymetry

Final Report

Prepared for:
Applied Oceanography and Geophysics Division
Ocean Science Directorate

DTIC

JUL 3 1 1985

A

R. Zollinger
A. Becker
F. Morrison

University of California
Berkeley, California 94704

DTIC FILE COPY

85     7     22     066

# Foreword

Airborne electromagnetic (AEM) systems have traditionally been used for detecting anomalous conductors in the earth. But as interpretation techniques improved, AEM systems have taken new roles in research.

This report describes an experimental evaluation of the concept of AEM. A special-purpose inversion algorithm was developed for determining seawater depths from AEM surveys, and the algorithm has proven itself to be fast, efficient, and highly stable.

R. P. Onorati, Captain, USN
Commanding Officer, NORDA

AD A 157 132

# REPORT DOCUMENTATION PAGE

| 1a. REPORT SECURITY CLASSIFICATION | 1b RESTRICTIVE MARKINGS |
|---|---|
| Unclassified | None |

| 2a. SECURITY CLASSIFICATION AUTHORITY | 3 DISTRIBUTION/AVAILABILITY OF REPORT |
|---|---|
| | Approved for public release; distribution is unlimited. |
| 2b. DECLASSIFICATION/DOWNGRADING SCHEDULE | |

| 4. PERFORMING ORGANIZATION REPORT NUMBER(S) | 5 MONITORING ORGANIZATION REPORT NUMBER(S) |
|---|---|
| NORDA Report 93 | NORDA Report 93 |

| 6 NAME OF PERFORMING ORGANIZATION | 7a. NAME OF MONITORING ORGANIZATION |
|---|---|
| Naval Ocean Research and Development Activity | Naval Ocean Research and Development Activity |

| 6c. ADDRESS (City, State, and ZIP Code) | 7b. ADDRESS (City, State, and ZIP Code) |
|---|---|
| Ocean Science Directorate NSTL, Mississippi 39529-5004 | Ocean Science Directorate NSTL, Mississippi 39529-5004 |

| 8a NAME OF FUNDING/SPONSORING ORGANIZATION | 8b OFFICE SYMBOL (If applicable) | 9. PROCUREMENT INSTRUMENT IDENTIFICATION NUMBER |
|---|---|---|
| Naval Ocean Research and Development Activity | | |

| 8c. ADDRESS (City, State, and ZIP Code) | 10. SOURCE OF FUNDING NOS. | | | |
|---|---|---|---|---|
| Ocean Science Directorate NSTL, Mississippi 39529-5004 | PROGRAM ELEMENT NO. | PROJECT NO. | TASK NO. | WORK UNIT NO. |
| | 63701 | 3201 | S-09 | 19 |

11 TITLE (Include Security Classification)
Data Analysis of Airborne Electromagnetic Bathymetry

12. PERSONAL AUTHOR(S)
R. Zollinger, A. Becker, and F. Morrison

| 13a TYPE OF REPORT | 13b. TIME COVERED | 14. DATE OF REPORT (Yr., Mo., Day) | 15. PAGE COUNT |
|---|---|---|---|
| Final | From _____ To _____ | April 1985 | |

16. SUPPLEMENTARY NOTATION

| 17. COSATI CODES | | | 18. SUBJECT TERMS (Continue on reverse if necessary and identify by block number) |
|---|---|---|---|
| FIELD | GROUP | SUB GR | Airborne electromagnetic bathymetry, magnetic fields, geology, |
| | | | |
| | | | |

19. ABSTRACT (Continue on reverse if necessary and identify by block number)

This report describes an experimental evaluation of the concept of airborne electromagnetic bathymetry. The airborne electromagnetic data that forms the basis of this project was contributed by Questor Surveys Ltd., Toronto, Canada. It was acquired with the Mark VI INPUT system along a 17-mile-long flight path off Cape Breton Island in the province of Nova Scotia. The water depth beneath the flight path ranged from 0 to more than 40 m.

| 20 DISTRIBUTION/AVAILABILITY OF ABSTRACT | 21 ABSTRACT SECURITY CLASSIFICATION |
|---|---|
| UNCLASSIFIED/UNLIMITED ☐  SAME AS RPT ☒  DTIC USERS ☐ | Unclassified |

| 22a NAME OF RESPONSIBLE INDIVIDUAL | 22b TELEPHONE NUMBER (Include Area Code) | 22c. OFFICE SYMBOL |
|---|---|---|
| J. A. Ballard | (601) 688-4760 | Code 340 |

DD FORM 1473, 83 APR          EDITION OF 1 JAN 73 IS OBSOLETE

# Executive summary

This report describes an experimental evaluation of the concept of airborne electromagnetic bathymetry. The airborne electromagnetic data that forms the basis of this project was contributed by Questor Surveys Ltd., Toronto, Canada. It was acquired with the Mark VI INPUT system along a 17-mile-long flight path off Cape Breton Island in the province of Nova Scotia. The water depth beneath the flight path ranged from 0 to more than 40 m.

A special-purpose inversion algorithm was developed for automatically determining seawater depths from the digital tapes that contain the flight data. The algorithm has proven itself to be fast, efficient, and highly stable. Its efficiency is best demonstrated by the low computing costs that, on a CDC 7600 computer, amount to about 5 cents/mile. Although the algorithm is based on a one-dimensional model of the water-rock interface, it was able to follow reasonably sharp sea-bottom topography. One of the main features of the algorithm, however, is its relative insensitivity to aircraft altitude and normal variations in the survey equipment configuration. This aspect is clearly demonstrated by the consistency in the depths obtained from four different data sets acquired at various elevations over the same flight path.

The average absolute error in the depth estimates derived from the electromagnetic data was about 2 m. As the discrepancies between the interpreted depths and the soundings shown on the coastal charts are not systematic, it is most likely that they are related to the presence of electrically conductive bottom sediments. It also appears that the value of 4 siemens/meter taken as the conductivity of sea water is essentially correct.

i

# Acknowledgments

# Contents

iii

# Data analysis of airborne electromagnetic bathymetry

## Introduction

Airborne electromagnetic (AEM) systems consist of a primary field source (transmitter) that produces a time-dependent magnetic field and a detector (receiver) that senses the secondary magnetic field produced by eddy currents induced in the earth. The first AEM system was developed 25 years ago in Canada for use in mineral exploration. Since then a large variety of AEM systems have been put into production, but most of these have now been abandoned for one reason or another. When the state of the art in this field was last reviewed (Becker, 1979), nearly a dozen different systems were available for commercial work. At present, this number has basically been reduced to two AEM systems: the time domain INPUT system, which is used in about 70% of surveys worldwide, and the towed rigid-boom helicopter frequency domain system, which accounts for an additional 25% of the work. The remaining 5% of the surveys are done with special-purpose and experimental systems.

AEM systems have traditionally been used for detecting anomalous conductors in the earth. Recently, as more quantitative interpretation techniques have evolved, some systems have also been used for mapping ground conductivity. Dyck et al. (1974), and more recently Whitting (1983), used the towed-bird INPUT transient system for mapping surficial sediment conductivity in Ontario. Fraser (1978) has described a helicopter EM system (Dighem) used for making resistivity maps. Pitcher et al. (1980) used a three-frequency, fixed-wing system to map overburden and delineate a lignite deposit. The INPUT studies are particularly relevant to the present investigation, since they demonstrate that accurate measurements of thickness and conductivity may be made for a highly conductive clay layer.

Two more studies of interest to this investigation include one by Glenn et al. (1973), which demonstrates that secondary electromagnetic fields may be used to uniquely determine the conductivity and thickness of a conducting surface layer, and one by DeMoully and Becker (1984), which shows that INPUT data can be interpreted in terms of a simplified geologic section. The interpretation techniques used to determine geologic parameters from AEM data can easily be adapted for use in interpreting offshore surveys. The feasibility of using a conventional airborne electromagnetic system in bathymetry surveys was recently confirmed by Morrison and Becker (1982) in a report submitted to the Office of Naval Research. Their analysis of conventional survey systems shows that the INPUT system appears best suited to the task. Theoretically, it can resolve a 40-m depth to better than 3% and a 60-m depth to about 15% when using an equivalent fundamental frequency of 144 Hz. Better resolving power may be obtained by using the modified INPUT system, which operates at a fundamental frequency of 90 Hz (a transmitter on-time of 2 msec).

The INPUT (Induced Pulse Transient) system was invented over 20 years ago by A. R. Barringer (Barringer, 1962) and has been modified a number of times since it was first rendered operational. In its present configuration, INPUT uses a high-power, 2-msec pulse to induce transient eddy currents in the ground. The secondary magnetic field generated by the decaying eddy currents is measured while the primary field is off by a receiver that is towed approximately 97 m behind and 67 m below the transmitter. Measuring the secondary fields in the absence of strong primary fields, a major advantage of all time domain methods, avoids electrical dynamic range problems and allows the use of a towed-bird receiver because a fair amount of receiver motion with respect to the aircraft will not cause any serious degeneration of signal quality. The secondary field transient is sampled a number of times after the cessation of the primary field (Fig. 1). Each sample is then fed to one of the six detector channels, and these are averaged over about 1 sec, or 180 repetitions of the primary pulse. The value of each channel is then displayed in parts per million of the peak primary receiver voltage on an analog record as a function of distance along the flight path (Fig. 2).

## Interpretation of offshore INPUT data

The huge amount of data collected in an AEM survey makes classical inversion techniques expensive and impractical. Instead, we have developed a fast, automatic curve fitting routine that analyzes offshore INPUT data by comparing it to theoretical results obtained for the INPUT system over a simple two-layer model (Fig. 3). In generating

1

this theoretical data, only two parameters of the model are varied; the seawater depth, $D$, and the height of the system over the water, $H$. The conductivity of the water is taken to be 4.0 siemens/meter (S/m), and the underlying halfspace is assumed to be almost infinitely resistive with a conductivity of 0.0001 S/m. In practice, $H$ is recorded by an altimeter during the survey, and this information may be used in the curve-fitting routine so that the seawater depth, $D$, is the only variable that remains to be determined.

In constructing tables of theoretical data used by the curve-fitting algorithm, transient decay curves are first computed for a variety of seawater depths and transmitter heights. Transients that would be measured by a system flying 230 m above a layer of seawater 0.5, 10, 30, and 100 m deep are shown in Figure 4. Notice that the amplitude of the transient, plotted logarithmically, is in parts per million of the peak voltage measured at the receiver while the primary field is on. The INPUT system is designed to sample the decaying amplitude of transients like these at the six times indicated on the horizontal axis.

Modeling reveals that slight changes in the system's altitude, up to about 10 m, raise or lower the amplitude of the whole transient without significantly changing its shape. However, changing $H$ by more than 10 m also introduces noticeable changes in transient shape that appear in the INPUT data as changes in the relative amplitudes of the six channels. Unless changes in aircraft elevation are taken into account, these relative variations in channel amplitudes could be mistakenly attributed to changing seawater depth. Complete sets of theoretical decay curves for 0.5-100 m of seawater are, therefore, generated for varying transmitter heights at 15-m intervals within the range of possible altitudes. The field data may then be fitted with the appropriate theoretical data based on the corresponding altimeter information. Before fitting field data to the theoretical curves, however, any overall shifts in the transient amplitude caused by small altitude fluctuations or by "bird swing" (slight changes in the relative positions of the transmitter and receiver) must be removed. This removal may be done by dividing the amplitude of the transient at each time by its amplitude at a fixed reference time, which leaves the relative channel amplitudes unaltered. Since the INPUT system measures the transient at six times, one of these times could be selected as the reference and all six channels could be normalized by the reference channel amplitude. This procedure, however, propagates the random noise of the normalizing channel throughout the other five channels. A better way to normalize the INPUT data is to divide each of the channels by the geometric mean amplitude

of channels 3 and 4 (Fig. 5). Using a combination of two channels to normalize all six channels reduces the chance of contaminating the data.

In Figure 6, the six theoretical normalized channel amplitudes are displayed individually as six curves, and the variation of each channel's amplitude with the increasing seawater depth is shown. Channels 3 and 4 are, of course, distributed symmetrically around 1.0, since they have been normalized by their geometric mean, or rather, by the average of their logarithms.

$$a = Geometric\ Mean\ of\ Channels\ 3\ and\ 4$$

$$= \sqrt{Ch(3)\,{}^*Ch(4)}$$

$$log\ a = \frac{log\ (Ch(3))\ +\ log\ (Ch\ (4))}{2}$$

Studying Figure 6 reveals that for each seawater depth the normalized transient may be described in terms of its early time amplitude and the degree of symmetry of the six normalized channels around 1.0. On this basis, the following two sums may be regarded as two characteristic quantities that, when used together, uniquely relate the six-channel INPUT data to seawater depth.

$$SUM(1) = \sum_{i=1}^{6} log\left(\frac{Channel\ (i)}{\sqrt{Ch(3)\,{}^*Ch(4)}}\right)$$

$$SUM(2) = \sum_{i=1}^{3} log\left(\frac{Channel\ (i)}{\sqrt{Ch(3)\,{}^*Ch(4)}}\right)$$

$SUM(1)$ is the sum of the logarithms of all the normalized channel amplitudes and, therefore, characterizes the symmetry of the curves around 1.0. In Figure 5, $SUM(1)$ $= a + b + c + d + e + f$. $SUM(2)$ is the sum of the logarithms of channels 1-3 and characterizes the early time amplitude of the normalized transient. In Figure 5, $SUM(2) = a + b + c$. Figure 7 shows how $SUM(1)$ and $SUM(2)$ change as the seawater depth increases from 0.5 to 100 m.

Now, instead of looking for the best fit between six channels of real data and six channels of theoretical data, two characteristic sums may be used to interpret offshore INPUT data. Additionally, since they depend on all six of the data channels, $SUM(1)$ and $SUM(2)$ are less sensitive to random noise than the channel amplitudes taken individually.

2

# Field example

The interpretation scheme developed in this investigation was tested on 100 miles of offshore INPUT data collected and made available to the University of California by Questor Surveys Ltd. of Toronto, Canada. All data was collected during six flights along a single 17-mile-long line that crosses the mouth of Lennox Passage near Cape Breton Island in Nova Scotia, Canada. The line was flown both east and west at altitudes of 550, 650, and 750 ft (170, 200, and 230 m) above sea level. Detailed bathymetry along the line, which is centered at 45°35'N, 60°50'W and runs N86°W, is available on Canadian Coastal Charts #4308 (1:37,500), #4275 (1:20,000), and #4279 (1:60,000).

The data collected while flying east at an altitude of approximately 230 m is displayed logarithmically in Figure 8. Notice that the six channels have been normalized by the geometric mean of channels 3 and 4. The western half of this record corresponds to the conventional INPUT record shown in Figure 2, in which the channels are plotted linearly in parts per million and where the zero ppm level for each channel is offset 300 ppm from that of the next channel. $SUM(1)$ and $SUM(2)$ are displayed at two locations along the line, points A and B, to demonstrate their use in interpreting the data in terms of seawater depth. These two points are also plotted on Figure 7, which is the appropriate interpretation chart for both of these places based on the corresponding altimeter record. This chart indicates that the seawater at points A and B is around 1.0 and 4.0 m deep, respectively. In the table used by the computer algorithm to interpret offshore INPUT data, the values of $SUM(1)$ and $SUM(2)$ are stored for every 1-m increase in depth for seawater 3–40 m deep. For shallower water this increment is reduced to 0.2–0.5 m, and in deeper water it is progressively increased from 2 to 10 m. For each data point along the flight line, the automatic interpretation algorithm calculates $SUM(1)$ and $SUM(2)$ from the six channels of EM data, selects the correct table of theoretical data based on the aircraft altitude, goes to the correct region of the table based on $SUM(1)$ and $SUM(2)$, and then compares the two calculated sums to each of 15 theoretical pairs of sums within that region. The seawater depth corresponding to the best fitting pair of theoretical sums is returned, along with an estimate of how well the real data fit the theoretical values. This process is accomplished quickly and inexpensively, costing about $0.05/mile ($0.05/105 data points) on a CDC7600 mainframe computer.

The results of this algorithm for the data set in Figure 8 are shown in Figure 9 where the interpreted depth profile is plotted with the corresponding known depth points taken from the coastal charts. The deep, narrow feature

at 12 km is the Lennox passage. The interpretation algorithm returns depths of 60-100 m for this feature, while the coastal charts put its maximum depth at 43 m. This range of depths corresponds to a very short segment of the curve in Figure 7, which supports the conclusions of Morrison and Becker (1982) that the ability of the INPUT system to resolve seawater depth is greatly reduced when depths exceed about 40 m.

In Figure 10, the interpreted results of four of the flights are displayed together on an expanded scale with the known bathymetry. Lines 13E and 14W were flown at 230 m, and Lines 15E and 16W were flown at 200 m above sea level (E and W designate the direction flown). The other two data sets, collected at an altitude of 170 m, were saturated on two to four channels in many places due to very high secondary field amplitudes. While these two data sets agreed with the other four in areas where no channels were saturated, they are not displayed in Figure 10.

The error between the interpreted depths from INPUT data and depths from coastal charts may be presented in three ways. The average error (AE) for a line is the sum of all the errors, positive and negative, divided by the number of points where the error may be calculated. The average error should approach zero if the errors are random. The average absolute error (AAE) is the sum of the absolute values of the errors divided by the number of points. The root-mean-square error (RMS) is the square root of the sum of the errors squared divided by the number of points and is essentially the standard deviation of the interpreted depths from the true depth.

$$Average\ Error = \frac{1}{N} \sum_{i=1}^{N} (D_{interpreted} - D_{known})$$

$$\begin{matrix} Average \\ Absolute \\ Error \end{matrix} = \frac{1}{N} \sum_{i=1}^{N} \left| (D_{interpreted} - D_{known}) \right|$$

$$\left[ \begin{matrix} Root\ Mean \\ Square\ Error \end{matrix} \right]^2 = \frac{1}{N} \sum_{i=1}^{N} (D_{interpreted} - D_{known})^2$$

For the four lines shown in Figure 10 the following errors were calculated.

|  | L13E | L14W | L15E | L16W |
|---|---|---|---|---|
| AE (m) | 0.415 | −0.271 | 0.327 | 0.001 |
| AAE (m) | 2.322 | 2.059 | 2.193 | 2.384 |
| RMS Error (m) | 3.071 | 2.548 | 2.977 | 2.920 |

From this calculation it may be seen that while the errors are random rather than systematic, an interpreted value for seawater depth is likely to be in error by an average of about 2 m or, alternatively, it probably falls within 3 m (one standard deviation) of the true depth.


# Source of errors

In addition to inescapable errors caused by random noise in the data, errors in interpreting seawater depths may be introduced by differences between reality and the parameters of the simplified model shown in Figure 1. The most obvious difference is that the seawater, in reality, is never an infinite layer of constant thickness. To model it as three dimensional, though, would be prohibitively expensive; the goal of this investigation is to obtain sufficiently accurate results using an inexpensive, simple model with very few degrees of freedom. Fortunately, the highly conductive seawater quickly attenuates the fields away from the transmitter so that lateral changes in seawater depth do not have a strong effect on the recorded transients. The errors introduced by modeling a three-dimensional seawater layer as one dimensional is not studied quantitatively in this investigation. Instead, the success achieved in mapping large gradients along the Cape Breton test line is empirical evidence that these errors are not substantial. Of interest to this investigation, however, are the errors that seawater or half-space conductivity changes would introduce and the effects of errors in transmitter altitude or transmitter-receiver configuration. While the errors introduced by additional fairly conductive layers (such as seabottom sediments) are of definite interest, a concurrent study by Turnross et al. (1984) investigates this at length. The general effects of intermediate layers will be discussed only briefly at the end of this section.

The errors caused by varying system parameters and conductivities were studied by generating theoretical data with parameters that differed from the model parameters and then inverting the data with the algorithm developed in this investigation.

## Changes in seawater conductivity

Varying the seawater conductivity ($\sigma(1)$) introduces, at most, an error due to changing the conductance (Conductivity * depth) of the seawater layer. For shallow sections in particular, small changes in $\sigma(1)$ do not have much effect on the conductance. When the inversion algorithm interprets this data, it sets $\sigma(1) = 4.0$ and adjusts the depth to match the conductance. Very little, if any, error is introduced in shallow depth estimates. The error intro-

duced in somewhat deeper water is $\leqslant \left(1 - \dfrac{4.0}{\sigma(1)}\right) * D$

where $\sigma(1)$ is the actual seawater conductivity, and $D$ is the interpreted depth. As the water becomes deeper, the error falls below this maximum as the seawater layer looks less and less like a thin sheet that can be characterized by its conductance. For example if $\sigma(1)$ varies from 4.0 S/m by ±0.1 S/m, no errors are introduced in the interpreted depths. For changes in $\sigma(1)$ of ±0.2 S/m, depths between 11 and 40 m will be in error by ±1 m and for changes in $\sigma(1)$ of ±0.4 S/m, depths between 5 and 24 m will be in error by ±1 m, and depths between 25 and 45 m will be ±2 m in error.

## Changes in half-space conductivity

Although the interpretation algorithm assumes a half-space conductivity, $\sigma(2)$, of 0.0001 S/m ($\varrho(2) = 10,000$ $\Omega m$), actual half-space conductivities up to 0.1 S/m ($\varrho(2) = 10\ \Omega m$) introduce, at most, 1 m of error in the interpreted depth profile (Fig. 11). Places where the seawater is around 10 m deep are most sensitive to the changes in $\sigma(2)$ and will be in error by 1 m as soon as $\sigma(2)$ is increased to 0.0005 S/m.

## Errors in transmitter altitude

Because the data is normalized in a way that removes the overall amplitude information from the transient, errors in the actual altitude of the transmitter introduce little or no error in the interpretation. If the altimeter were to record transmitter heights that were 10 m too high or too low when the aircraft was flying at 230 m above the seawater, the inversion algorithm would interpret the seawater depth correctly. If the recorded height of the transmitter was in error by 20 m, interpreted seawater depths between 5 and 12 m and from 24 to 25 m would be in error by ±1 m. If the recorded transmitter height was 30 m too high, interpreted depths from 2 to 13 m and from 21 to 27 m would be 1 m too high. If the recorded transmitter height was 30 m too low, the interpreted depths from 2 to 9 m and from 21 to 27 m would be 1 m too low, and depths between 10 and 14 m would be 2 m too low. These errors are relatively insignificant, especially since it is unlikely that the altimeter information could be wrong by 10 m, much less 30 m. However, it illustrates the insensitivity of this technique to small changes in transmitter height and confirms that this algorithm could not be used in areas of known seawater depth to check the altimeter data.

## Errors in transmitter-receiver configuration

Because the receiver is towed behind the aircraft on 400 ft of cable, the actual position of the receiver depends on aircraft speed, wind, and turbulence. Changes in this configuration, often called "bird swing," can cause interpretation errors. The algorithm developed in this investigation assumes that the bird (receiver) is 97 m behind and 67 m below the aircraft, its approximate position when the plane is flying 110 knots. In this position, the receiver is $35^0$ below a horizontal plane through the transmitter. Modeling shows that over a reasonable range of bird swing, errors introduced in the interpretation are entirely insignificant. If the bird swings upward $5^0$ ($30^0$ below the aircraft), the interpreted depth over 12 m of seawater will be 1 m too low, and over 37 m of water will be 1 m too high. If the bird swings downward $5^0$ ($40^0$ below the receiver), the interpreted depth over 12, 37, or 39 m of water will be 1 m too low. Only these isolated depths are sensitive to the effects of bird swing; other depths of seawater from 0.5 to 70 m will be interpreted correctly.

## Effect of intermediate layers

A thin layer of intermediate conductivity between the seawater layer and the half-space (representing, for example, seabottom sediments) tends to increase the conductance of the whole section above the half space, thereby creating an apparent increase in the seawater depth. For example, 10 m of a conductive mud ($\sigma = 1.0$ S/m) has a conductance of 10.0 S. Interpreted as an equivalent layer of seawater ($\sigma = 4.0$ S/m), the mud will simply look like an additional 2.5 m of water. A thick layer of intermediate conductivity introduces much less error than a thin layer, as currents induced in it spread downward and farther away from the receiver. In the limit that the thick layer looks like a half-space to the system, the errors introduced

by it approach the half-space errors outlined in Figure 11. The point at which the layer ceases to be "thin" (introducing an error that increases as its conductivity-thickness product increases) and becomes "thick" (introducing progressively less error until it reaches the half-space error) is open to interpretation. The maximum thickness of a "thin" layer is around 10% of the height of the transmitter above it. A rigorous study of the effect of intermediate layers on the interpretation of offshore AEM data was made by Turnross et al. (1984).

## Conclusions

Using a simple two-layer model, interpreting offshore INPUT data in terms of seawater depth quickly, inexpensively, and accurately is possible. A test case showed that over 0-40 m of seawater, the average error between the interpreted depths and known depths recorded by traditional bathymetric soundings is about 2 m. Sharp depth gradients were resolved accurately, and independent interpretations of data sets collected at different altitudes and in different directions show excellent repeatability. The inversion algorithm developed is very stable; it displays low sensitivity to the effects of reasonable changes in seawater conductivity, half-space conductivity, system altitude, and transmitter-receiver configuration. The stability of the algorithm and its ability to resolve lateral gradients, which clearly contradict the one-dimensional forward model, may be attributed to the high conductivity of seawater. Eddy currents are easily induced in the saline water, generating strong localized secondary fields that mask any other effects due to small variations in the real world. This suggests that the algorithm developed in this paper cannot be used for determining the seawater salinity, the properties of bottom sediments, or the half-space conductivity.

# References

Barringer, A. F. (1962). The INPUT Electrical Pulse Prospecting System. *Min. Cong. Journal*, v. 48, pp. 49-52.

Becker, A. (1979). Airborne Electromagnetic Methods, Geophysics, and Geochemistry in the Search for Metallic Ores. In: *Economic Geology Report* 31, Peter J. Hood (ed.), Geological Survey of Canada, pp. 33-43.

DeMoully, G. T. and A. Becker (1984). Automated Interpretation of Airborne Electromagnetic Data. *Geophysics*, v. 49, pp. 1301-1312.

Dyck, A. F., A. Becker, and L. S. Collett (1974). Surficial Conductivity Mapping with the Airborne INPUT System. *CIMM Bulletin*, v. 66, pp. 104-109.

Fraser, D. C. (1978). Resistivity Mapping with an Airborne Multicoil Electromagnetic System. *Geophysics*, v. 43, pp. 142-172.

Glenn, W. E., J. Ryu, S. H. Ward, W. J. People, and R. J. Phillips (1973). The Inversion of Vertical Magnetic Dipole Sounding Data. *Geophysics*, v. 38, pp. 1109-1129.

Morrison, H. F. and A. Becker (1982). *Analysis of Airborne Electromagnetic Systems for Mapping Depth of Seawater*. Final report, Office of Naval Research, Washington, D.C., Contract #N00014-82-M-0073, pp. 1-57.

Pitcher, D. H., R. B. Barlow, and M. Lewis (1980). Tridem Airborne Conductivity Mapping as a Lignite Exploration Method. *CIMM Bulletin*, May, pp. 1-12.

Turnross, J., H. F. Morrison, and A. Becker (1984). *Analysis of Airborne EM Systems for Mapping Conductivity and Thickness of Bottom Sediments: Part II: Analysis of Uniform vs. Gradational Conductivities*. Final report, Office of Naval Research, Washington, DC, Contract #N00014-84-K-0691.

Whiting, T. H. (1983). Surficial Conductivity Mapping with INPUT Airborne EM System and Its Application to Coal Exploration. Proceedings, *4th International Coal Symposium*, Sydney, N.S.W. Australia, 17 pp.
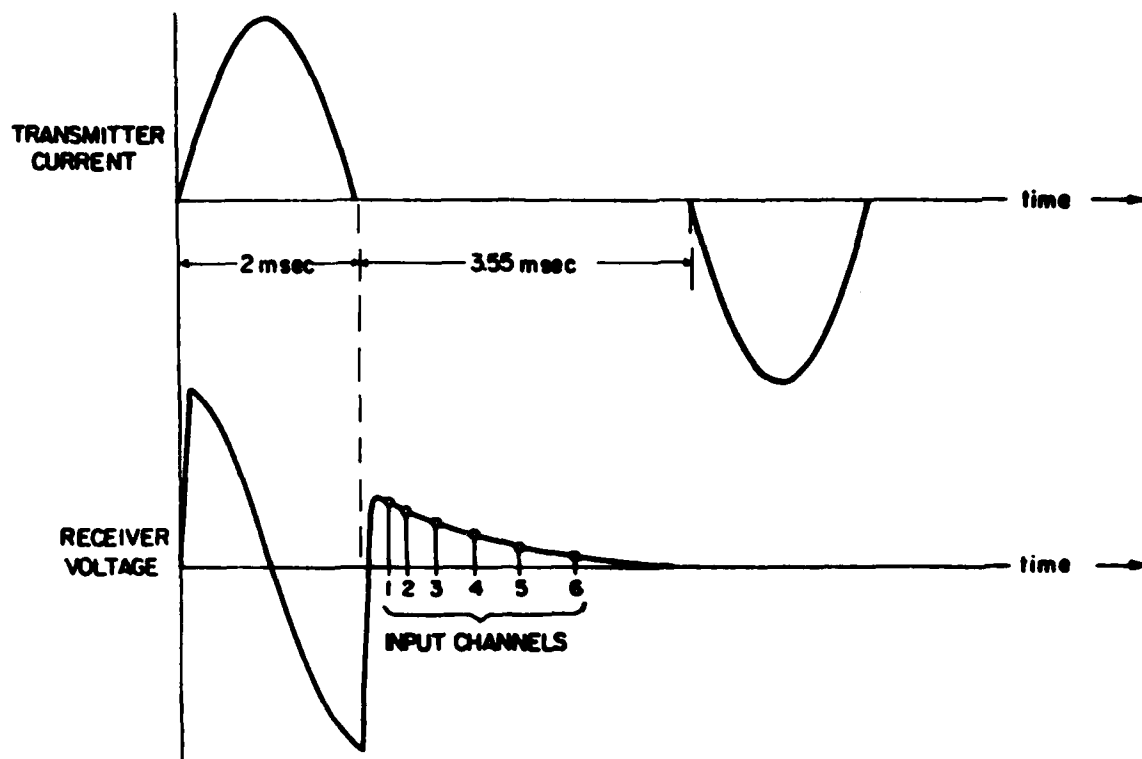
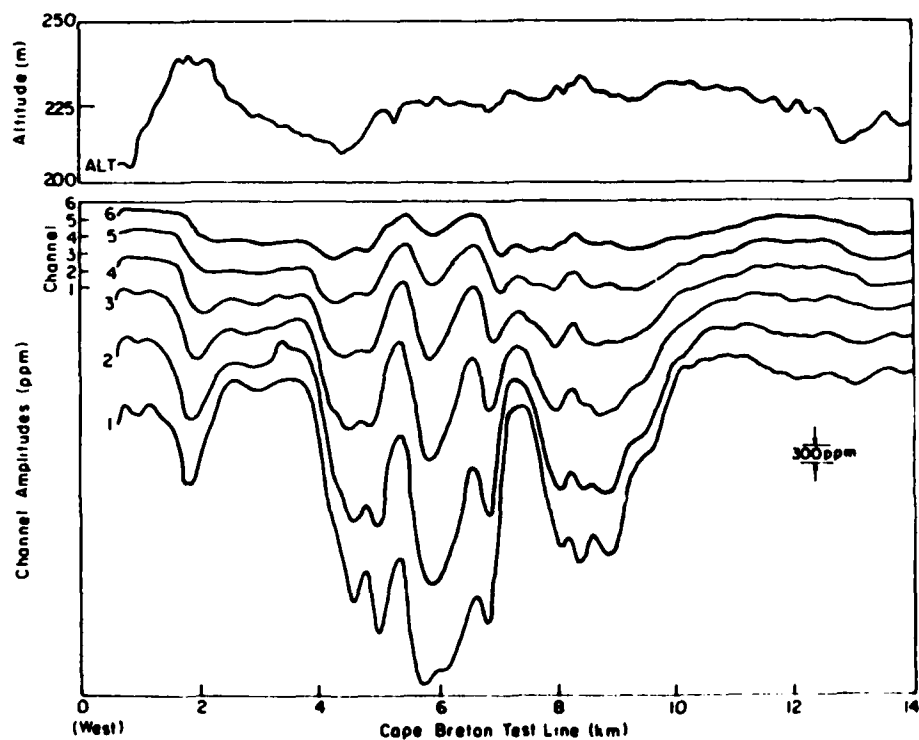Figure 1. *The transmitter waveform and corresponding receiver voltage for the INPUT system.*



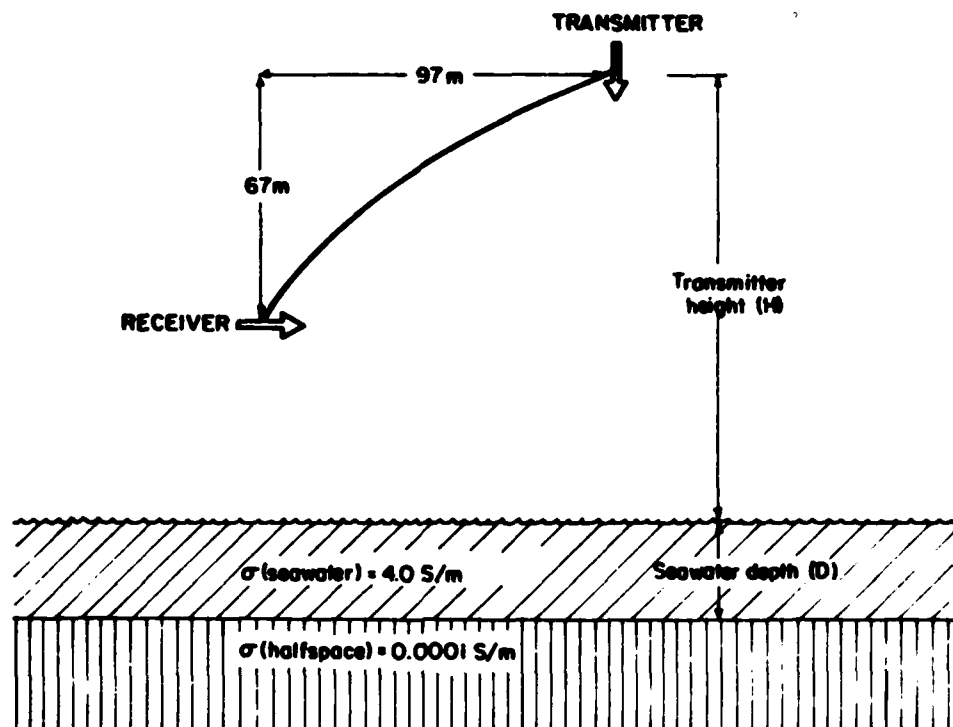Figure 2. *A conventional INPUT record with the horizontal scale compressed.*

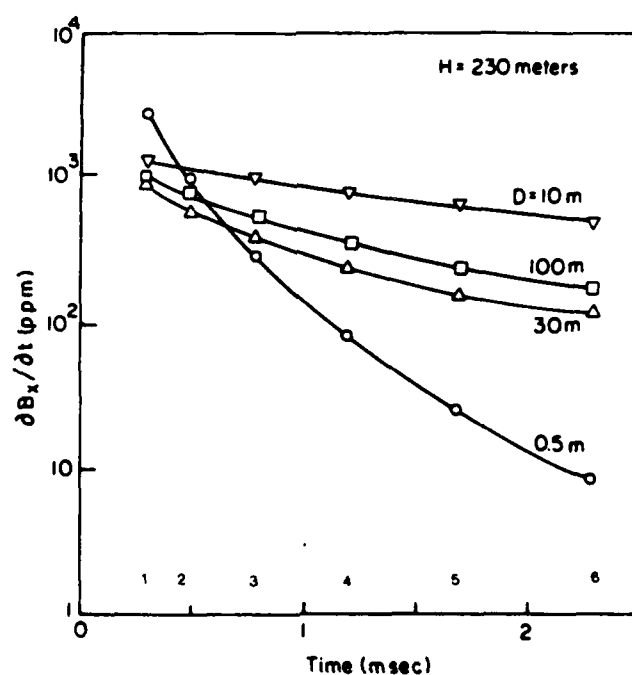Figure 3. Model parameters and system geometry.



Figure 4. Transients that would be measured by the INPUT system 230 m above seawater that is 0.5, 10, 30, and 100 m deep. The location of the six channels is shown on the time axis.
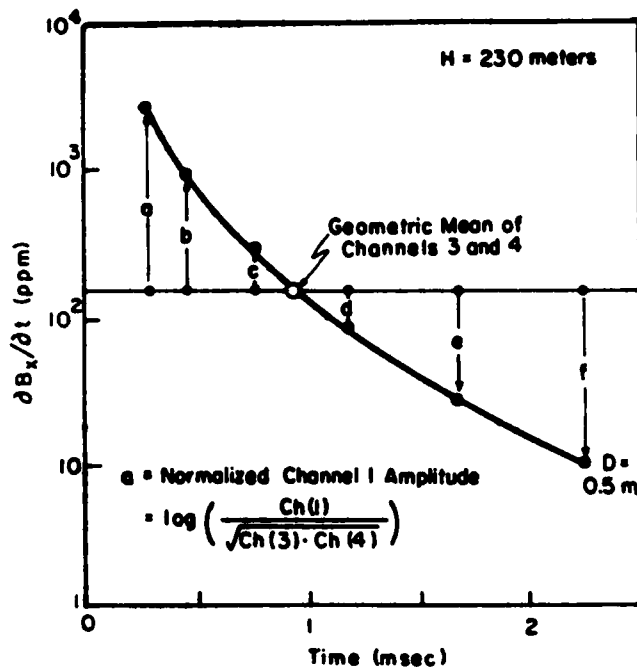
8

Figure 5. *The transient measured 230 m above 0.5 m of
seawater with the geometric mean amplitude of channels 3
and 4 labeled.*

$$SUM(1) = a + b + c + d + e + f$$
$$SUM(2) = a + b + c$$
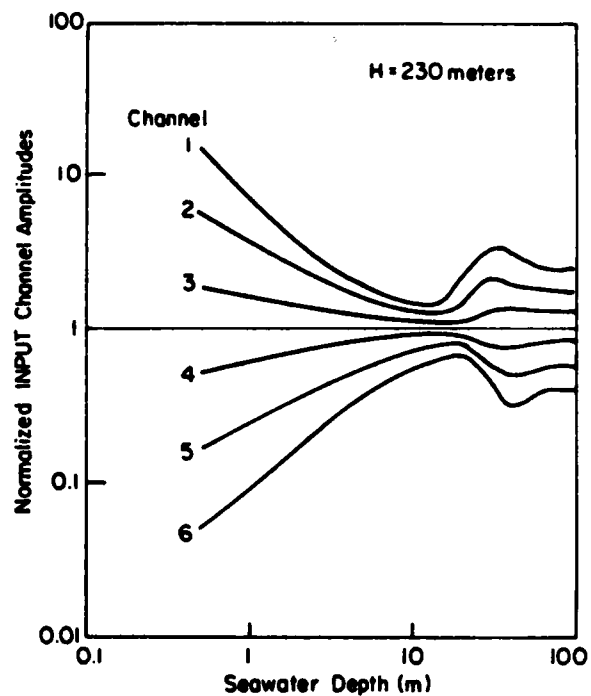


Figure 6. *The variation of channel amplitudes with the depth
of seawater. The channel amplitudes have been normalized
by the geometric mean of channels 3 and 4.*
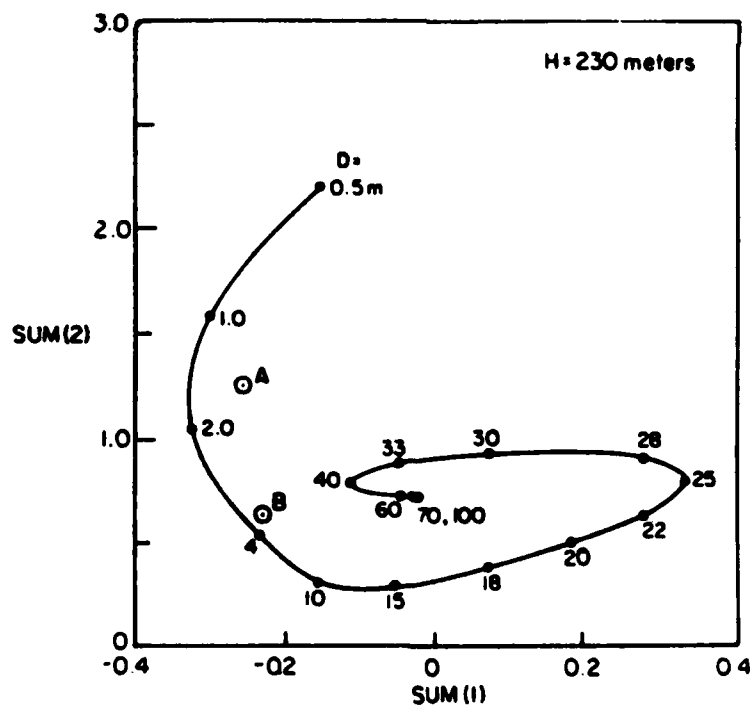


Figure 7. *The variation of SUM(1) and SUM(2) as seawater
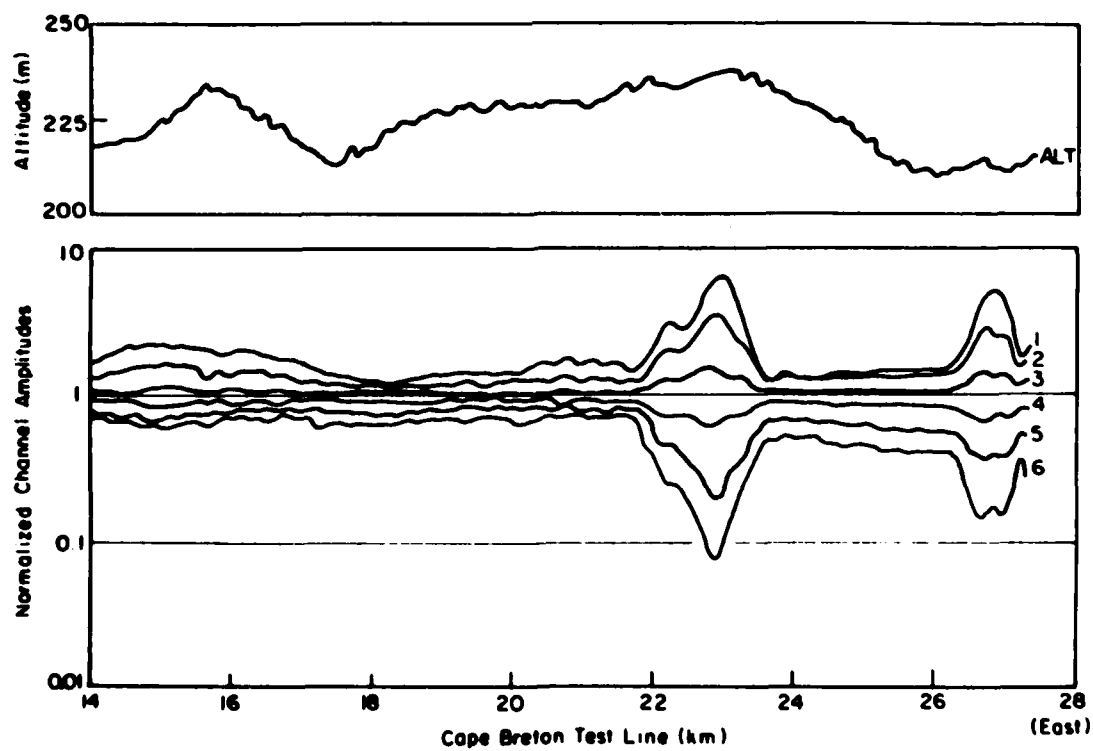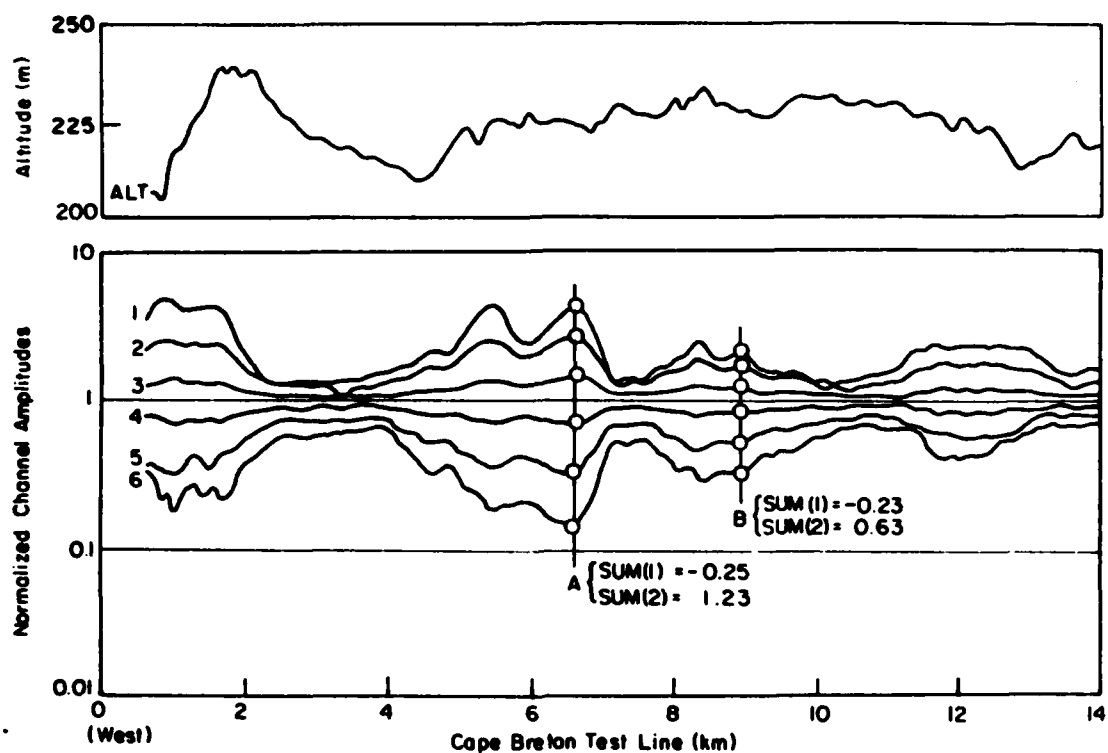depth increases from 0.5 to 100 m.*

9

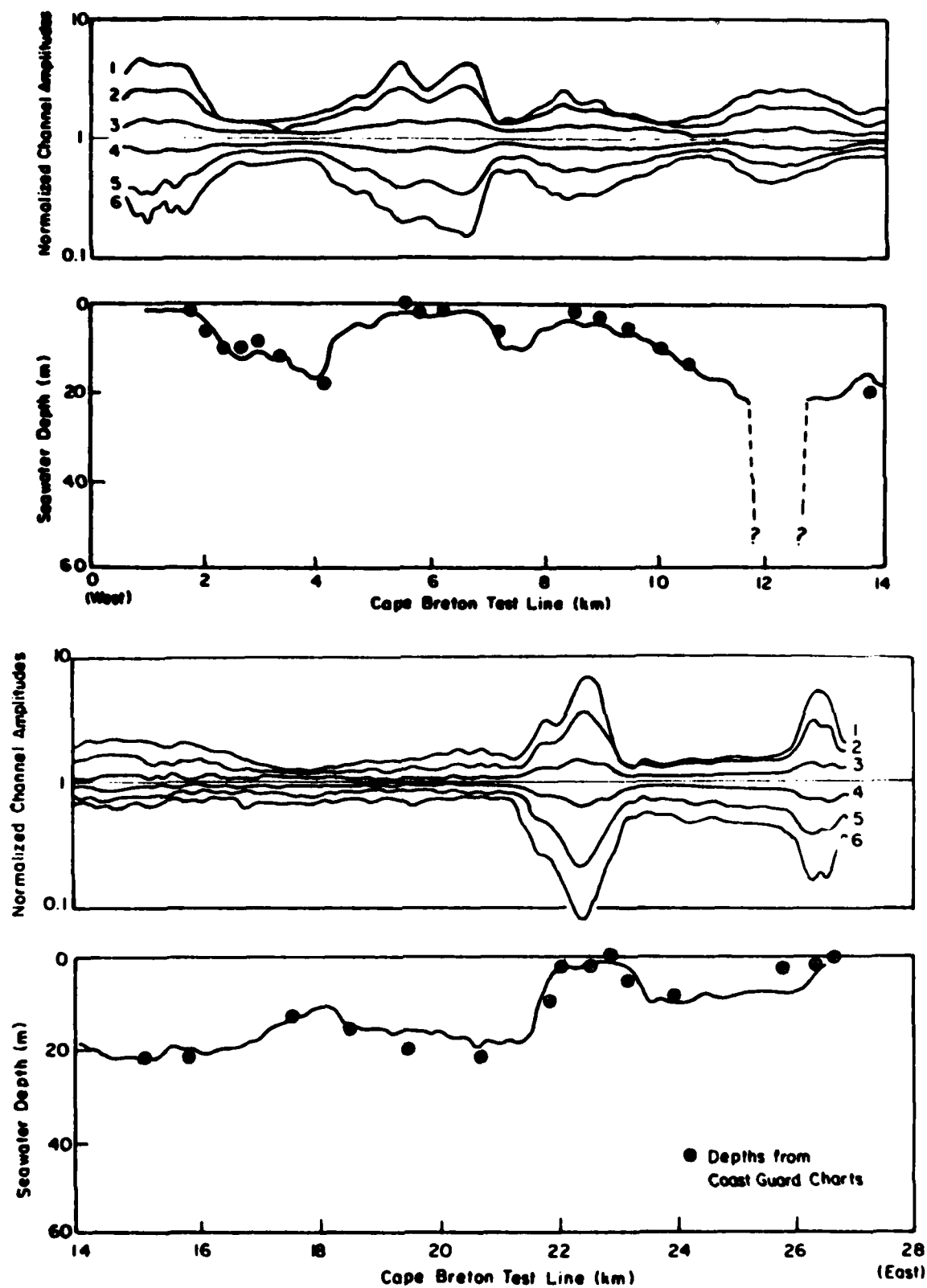*Figure 8 INPUT data from Nova Scotia, Canada.*

10

*Figure 9. Interpreted INPUT data from Nova Scotia with corresponding bathymetry from Coastal Charts.*
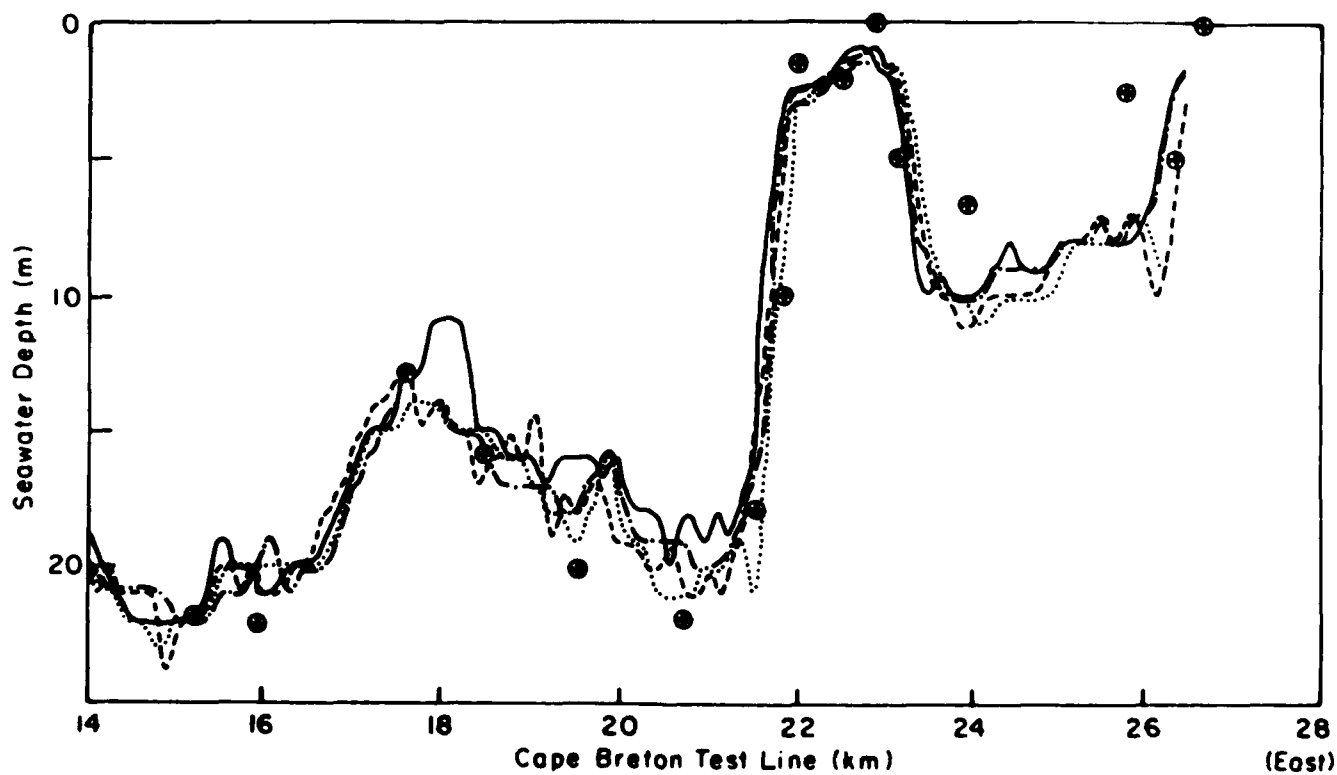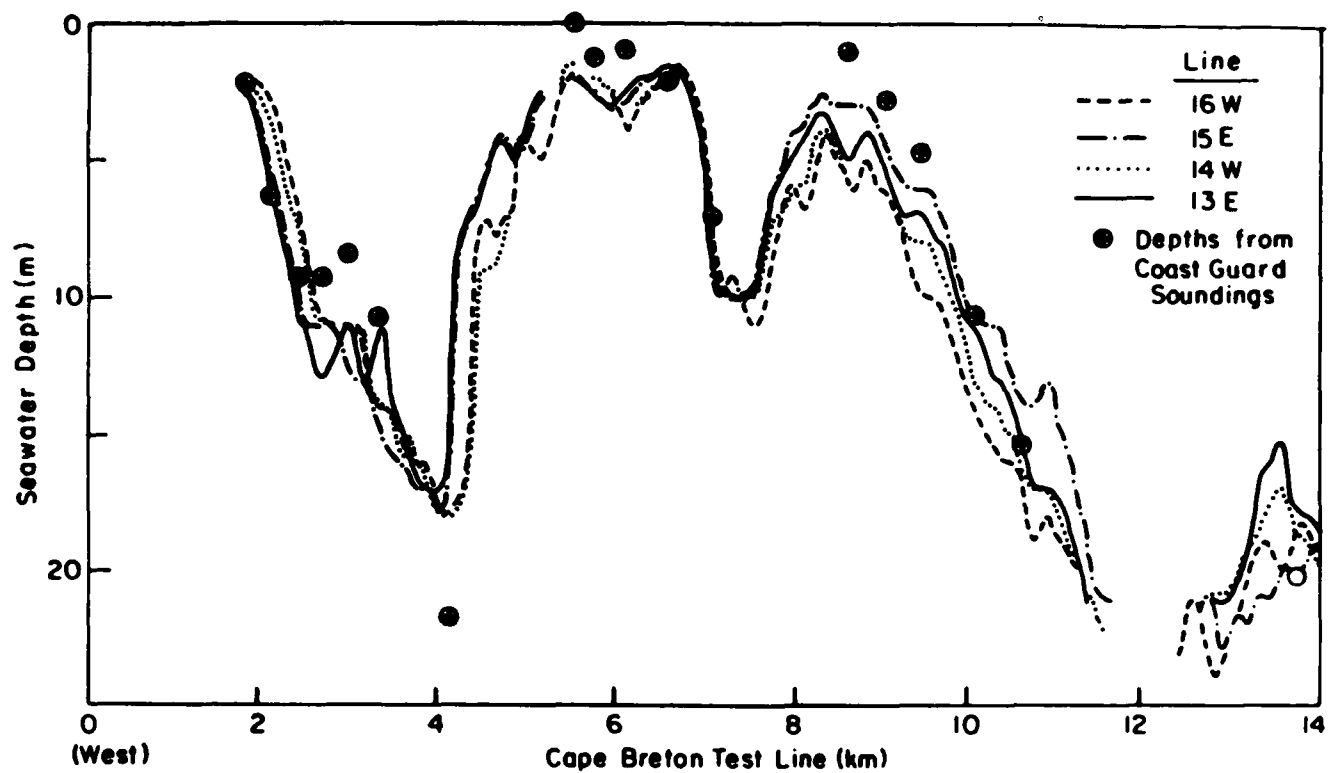
11

*Figure 10. A compilation of the results of interpreting four different INPUT data sets collected along the same line.*
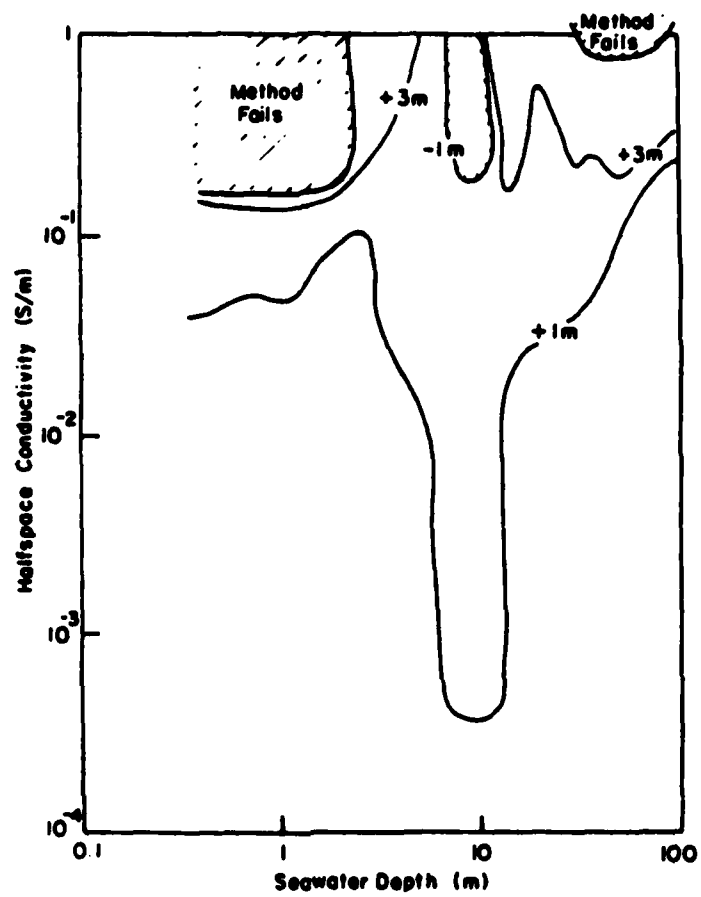
*Figure 11. The error introduced by changing the half-space conductivity.*

13

Distribution List

Department of the Navy
Asst Secretary of the Navy
(Research Engineering & System)
Washington DC 20350

Department of the Navy
Chief of Naval Operations
ATTN: OP-951
Washington DC 20350

Department of the Navy
Chief of Naval Operations
ATTN: OP-952
Washington DC 20350

Department of the Navy
Chief of Naval Operations
ATTN: OP-987
Washington DC 20350

Department of the Navy
Chief of Naval Material
Washington DC 20360

Commander
Naval Air Development Center
Warminster PA 18974

Commander
Naval Air Systems Command
Headquarters
Washington DC 20361

Commanding Officer
Naval Coastal Systems Center
Panama City FL 32407

Commander
Naval Electronic Systems Com
Headquarters
Washington DC 20360

Commanding Officer
Naval Environmental Prediction
Research Facility
Monterey CA 93940

Commander
Naval Facilities Eng Command
Headquarters
200 Stovall Street
Alexandria VA 22332

Commanding Officer
Naval Ocean R & D Activity
ATTN: Codes 100/105/110/111/112
113/115/125L/125P/200/300
NSTL MS 39529

Commanding Officer
Naval Research Laboratory
Washington DC 20375

Commander
Naval Oceanography Command
NSTL MS 39529

Commanding Officer
Fleet Numerical Ocean Cen
Monterey CA 93940

Commanding Officer
Naval Oceanographic Office
NSTL MS 39522

Commander
Naval Ocean Systems Center
San Diego CA 92152

Commanding Officer
ONR Branch Office LONDON
Box 39
FPO New York 09510

Officer in Charge
Office of Naval Research
Detachment, Pasadena
1030 E. Green Street
Pasadena CA 91106

Commander
Naval Sea System Command
Headquarters
Washington DC 20362

Commander
D W Taylor Naval Ship R & D Cen
Bethesda MD 20084

Commander
Naval Surface Weapons Center
Dahlgren VA 22448

Commanding Officer
Naval Underwater Systems Center
ATTN: NEW LONDON LAB
Newport RI 02841

Superintendent
Naval Postgraduate School
Monterey CA 93940

Project Manager
Chief of Naval Material
Department of the Navy
Washington DC 20360

Department of the Navy
Deputy Chief of Naval Material
for Laboratories
Rm 866 Crystal Plaza Five
Washington DC 20360

Officer in Charge
Naval Underwater Sys Cen Det
New London Laboratory
New London CT 06320

Defense Technical Info Cen
Cameron Station
Alexandria VA 22314

Director
Chief of Naval Research
ONR Code 420
NSTL MS 39529

Director, Liaison Office
Naval Ocean R & D Activity
800 N. Quincy Street
Ballston Tower #1
Arlington VA 22217

Department of the Navy
Office of Naval Research
ATTN: Code 102
800 N. Quincy Street
Arlington VA 22217

Director
Woods Hole Oceanographic Inst
86-96 Water St.
Woods Hole MA 02543

Director
University of California
Scripps Institute of Oceanography
P. O. Box 6049
San Diego CA 92106

Working Collection
Texas A & M University
Department of Oceanography
College Station TX 77843

# END

# FILMED

9-85

# DTIC